Suppressed piezoelectric polarization in single InGaN/GaN heterostructure nanowires

Wen-Che Tsai,[1] Yen-Ting Chen,[2] Chia-Hsien Lin,[1] Wei-Ting Hsu,[1] Yung-Sheng Hsu,[1] Li-Chyong Chen,[2] Kuei-Hsien Chen,[3] and Wen-Hao Chang[1,*]

[1]*Department of Electrophysics, National Chiao Tung University, Hsinchu 30010, Taiwan*
[2]*Center for Condensed Matter Sciences, National Taiwan University, Taipei 10617, Taiwan*
[3]*Institute of Atomic and Molecular Sciences, Academia Sinica, Taipei 10617, Taiwan*

(Received 29 August 2013; revised manuscript received 10 October 2013; published 28 October 2013)

The optical properties of single InGaN/GaN heterostructure nanowires (NWs) with a mean diameter down to 18 nm are investigated. Sharp emission lines originating from the recombination of localized excitons in the InGaN disk layer can be resolved. Excitation-dependent energy shifts, together with spectral diffusions of these emission lines, indicate the presence of a weak quantum confined Stark effect (QCSE) caused by nearby charge fluctuations, rather than the screening of piezoelectric polarizations at the InGaN/GaN interface. The absence of a piezoelectric polarization field is further confirmed by time-resolved photoluminescence measurements. Numerical simulations reveal that the elastic strain relaxation via the NW geometry is marginal and occurs only near the NW sidewalls. Carrier localization preferentially near the periphery of the InGaN disk and alloy intermixing are suggested as possible reasons for the absence of a polarization-induced QCSE in thin InGaN/GaN heterostructure NWs.

DOI: 10.1103/PhysRevB.88.155323 PACS number(s): 78.67.Lt, 78.55.Cr

I. INTRODUCTION

Group-III nitrides have been recognized as an important material for various electronic and optoelectronic devices.[1,2] Of particular importance is the InGaN ternary alloy due to its adjustable band gap from the near ultraviolet to near infrared.[3,4] However, the internal quantum efficiency is limited by the presence of spontaneous and piezoelectric (strain-induced) polarizations at the InGaN-GaN heterointerface, leading to a large electric field (typically up to MV/cm) exhibited in the InGaN layer. The large built-in electric field gives rise to a strong quantum confined Stark effect (QCSE), which tends to redshift the emission energy, separate the electron and hole wave functions, and hence reduce the oscillator strength of the optical transition.

Recently, one-dimensional InGaN/GaN heterostructures formed by GaN nanocolumns or nanowires (NWs) with InGaN disk insertion layers[5–10] have been proposed to tackle this problem. Indeed, the absence of excitation-induced blueshift has been observed in either ensemble or single InGaN/GaN NWs.[8–12] The insignificant piezoelectric polarization field was attributed to efficient strain relaxation via the NW sidewalls. On the other hand, recombination lifetime reductions accompanied by small excitation-induced blueshifts ($\sim$1–10 meV) have been observed, indicating the presence of a weak piezoelectric polarization field in InGaN/GaN nanocolumns.[13,14] Numerical simulations based on the finite element method (FEM), combined with a detailed structural analysis of various InGaN/GaN NW heterostructures, however, suggested that the NW geometry only accommodates marginal elastic relaxations; rather strong piezoelectric polarizations still reside in the InGaN disk.[14–16] This inconsistency has yet to be clarified. For GaN/(Al,Ga)N NW heterostructures, the impact of stain and polarization on their optical properties has also been intensively studied.[17–20] It is quite convincing that GaN/AlN NWs are subject to the polarization-induced QCSE, although the magnitude is reduced somewhat by the size-dependent elastic strain relaxation via the NW geometry.[17,18,20] However, this picture for InGaN/GaN NWs is further complicated by the presence of carrier localization centers, which is commonly seen in InGaN ternary alloys.[21,22] Recently, a green emission band that exhibits strong excitation-induced blueshifts and a number of sharp emission lines with peak energies insensitive to excitation density were found to coexist in the spectra of single InGaN/GaN NWs.[16] It was argued that strong carrier localizations may be the origin for the absence of the QCSE for those sharp emission lines.[16]

In the present paper, we report on microphotoluminescence (μPL) measurements on single InGaN/GaN NWs. Previous studies on single InGaN/GaN NWs are mostly with diameters ranging from 40 to 150 nm.[11–14,16] Here we investigate much thinner NWs with diameters in the range of 9–27 nm.[23] Sharp emission lines originating from the recombination of localized excitons in the InGaN disk layer can be resolved at low temperatures. Excitation-dependent energy shifts, spectral diffusions, and time-resolved PL measurements of these emission lines indicate that the piezoelectric polarization field is insignificant in InGaN/GaN heterostructures. Possible reasons for the absence of the polarization-induced QCSE in InGaN/GaN NW heterostructures are discussed.

II. EXPERIMENT

The InGaN/GaN NW heterostructures were grown on a Si(111) substrate by radio-frequency plasma assisted molecular beam epitaxy. After the growth of a thin AlN buffer layer, GaN NWs were grown at 750 °C under N-rich conditions (3.5 sccm). A 2-nm-thick InGaN layer followed by a 5-nm-thick GaN capping layer were then grown on top of these NWs at the same temperature. The InGaN/GaN NW heterostructures have been analyzed by scanning electron microscopy (SEM), high-resolution transmission electron microscopy (HR-TEM) (JEOL JEM-2100, 200 kV), and accompanying scanning transmission electron microscopy with energy-dispersive x-ray (STEM-EDX) spectroscopy (Oxford INCATM Microsystem). Statistically, the average NW diameter is 18 nm and 9 nm is the minimum. The wire lengths can be distributed from 1 to 4 μm, depending on the growth time. Composition analysis

 ©2013 American Physical Society

using STEM-EDX spectroscopy indicates that the In content in the InGaN disk layer is about 10%. HR-TEM analysis near the InGaN disk layer reveals that the InGaN/GaN heterostructures are mostly defect free, i.e., without noticeable cracks and misfit dislocations. The details of the structural analyses can be found in Ref. 23.

Emission spectra of single InGaN/GaN NWs were measured by a low-temperature μPL setup. The measurements were carried out at $T \simeq 6$ K using the 325-nm line of a He-Cd laser as an excitation source. The laser was focused to a spot of about 1 μm in diameter by an objective lens (numerical aperture, NA = 0.5). The μPL signals were analyzed by a 0.75-m grating monochromator (1200 g/mm) and detected by a liquid-nitrogen-cooled charge-coupled device, which yields a spectral resolution of 0.05 nm (~400 μeV). For time-resolved PL measurements, the excitation source was replaced by a mode-locked Ti-sapphire laser, which is frequency doubled to a wavelength of 355 nm with a 200-fs pulse duration and 80-MHz repetition rate. The decay traces were detected by a fast avalanche photodiode and recorded using the time correlated single-photon-counting technique with a temporal resolution of ~150 ps. To assess the PL spectrum of single NWs, the deposited NWs were mechanically scratched from the substrate and then dispersed in methanol. The solution was then dropped onto another Si substrate with a gold pattern on top. After drying, single NWs were separately dispersed on the substrate.

III. RESULTS AND DISCUSSION

Figure 1 shows a typical μPL spectrum of a representative single NW measured at $T \simeq 6$ K under a cw excitation power of $P_{ex} = 40$ μW. Spectral features ranging from 3.3 to 3.5 eV are attributed to the near-band-edge emissions from the GaN NW. A number of sharp emission lines can be observed at energies below 3.2 eV. This spectral range corresponds to the low-energy side of the InGaN emission band observed in the NW ensemble. The linewidths of these emission lines range from 500 μW to ~1 meV. According to previous studies on InGaN/GaN quantum wells (QWs)[22] and quantum dots formed by self-assembled growth,[24–27] these sharp lines can be attributed to the emissions from localized excitons in the InGaN disk layer.[12] Although the diameter of the investigated NWs (9–27 nm) is quite small, it is still large in comparison with the exciton Bohr radius (~3 nm) in InGaN. In other words,

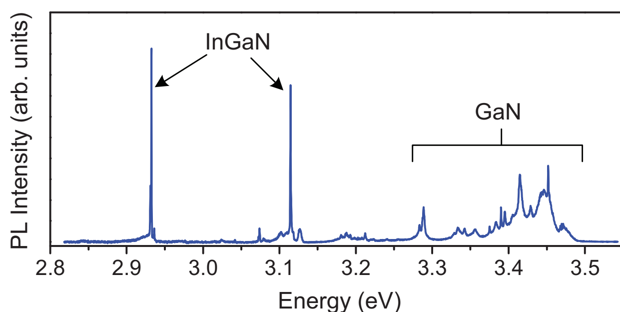

FIG. 1. (Color online) A typical μPL spectrum taken from a representative single InGaN/GaN NW.

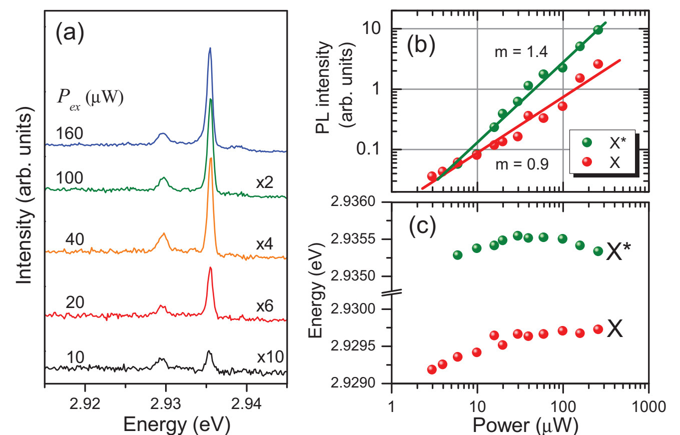

FIG. 2. (Color online) (a) Power-dependent PL spectra for the emission lines near 2.93 eV. (b) Integrated intensities and (c) peak energies of X and X^* lines as a function of excitation power.

the InGaN disk still acts somewhat as a QW without lateral quantum confinements. We have measured many individual NWs and found that the emission energies and the number of sharp lines vary from wire to wire. This indicates that the exciton localizations are likely to arise from some randomly distributed localization centers in the InGaN disk layer caused by local thickness and/or alloy fluctuations.

Figure 2(a) shows a series of PL spectra for the two emission lines near 2.93 eV (labeled as X and X^*) taken under different excitation powers. The integrated PL intensity I_{PL} as a function excitation power P_{ex} is displayed in Fig. 2(b). The power dependence of each line can be characterized by $I_{PL} \propto P_{ex}^m$, in which the exponent m is a fitting parameter. With increasing P_{ex}, the X line intensity increases almost linearly ($m \approx 0.9$), whereas the X^* line exhibits a superlinear power dependence ($m \approx 1.4$). The X line can thus be attributed to the recombination of single excitons, while the X^* line is likely to arise from charged excitons.[28] We note that there is no apparent intensity saturation for both X and X^* lines. This is limited by the maximum attainable laser power of our measurement system for this particular NW. Intensity saturation as well as biexciton lines are indeed observed in different NWs.[23] In fact, the spectral features (i.e., excitonic species and the in-between energy separations) of different localization centers are found to vary from NW to NW. Unlike self-assembled quantum dots, there is no similar potential profile for these localization centers induced by local alloy and/or thickness fluctuations in the InGaN layer. Therefore, it is unlikely for one to find a similar spectral pattern among different localization centers in different NWs.

In Fig. 2(c), the emission energies of X and X^* lines are plotted as a function of P_{ex}. Only a very small blueshift of ~0.46 meV is observed for the X line when the excitation power is increased from 3 to 30 μW. In conventional InGaN/GaN QWs, the presence of a strong built-in electric field (~MV/cm) induced by piezoelectric polarizations[29] can lead to an excitation-induced blueshift up to a few tens or even hundreds meV's due to the screening of the QCSE by the photogenerated carriers. The observed small excitation-induced blueshift is therefore a signature of suppressed piezoelectric

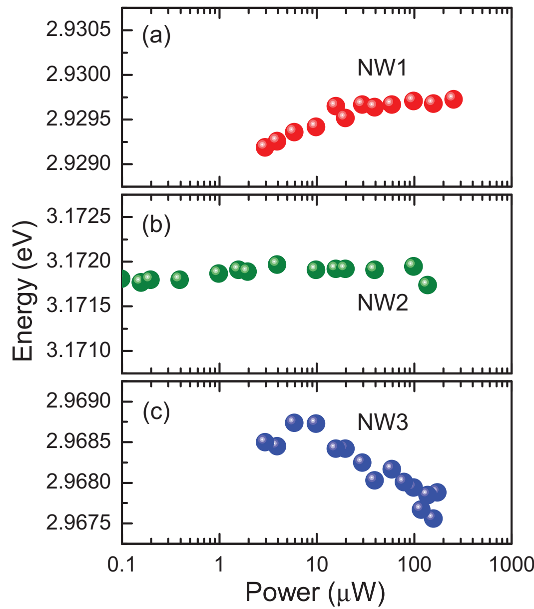

FIG. 3. (Color online) Peak energy as a function of excitation power for three different InGaN/GaN NWs.

polarizations in the investigated InGaN/GaN heterostructure NWs.

We have measured several NWs and analyzed the excitation-dependent spectra of emission lines from the InGaN disk layer. It was found that an energy blueshift with increasing excitation power is not a general trend. As shown in Fig. 3, blueshifted, redshifted, or even a constant peak energy with increasing excitation power can be observed in different NWs. This dependence is not anticipated from the screening of the QCSE caused by the piezoelectric polarization field in InGaN/GaN NWs. In addition, the energy shifts are quite small, typically smaller than the linewidth (<1 meV) of each emission line. Therefore, we suggest that the excitation-induced energy shift is related to the electric field produced by some charged traps in the vicinity of the exciton localization centers. Under optical excitations, the photogenerated carriers can either ionize or neutralize these traps and thereby the average electric field could be either increased or decreased by the increasing excitation power, depending on the initial charge states of these nearby traps.

The influence of the nearby charged traps can be studied by monitoring the spectral diffusions of these emission lines. Figure 4(a) shows the spectra of NW1 near the X and X^* lines recorded as a function of time with an integration time of 1 s for each. Although the influences of nearby traps that occur on a time scale shorter than 1 s are averaged, both the X and X^* lines reveal spectral diffusions with amplitudes $\lesssim$0.5 meV. A statistics of the nearly 800 consecutive spectra indicated that the integrated PL intensity and peak energy of X and X^* lines are correlated. As shown in Figs. 4(b) and 4(c), a blueshifted (redshifted) PL peak is accompanied by an enhanced (suppressed) PL intensity. This correlation clearly indicates that the spectral diffusion is caused by the QCSE arising from nearby charge fluctuations. In addition, we also found that the X and X^* lines exhibit the same spectral diffusion pattern. This is evident from the data shown in

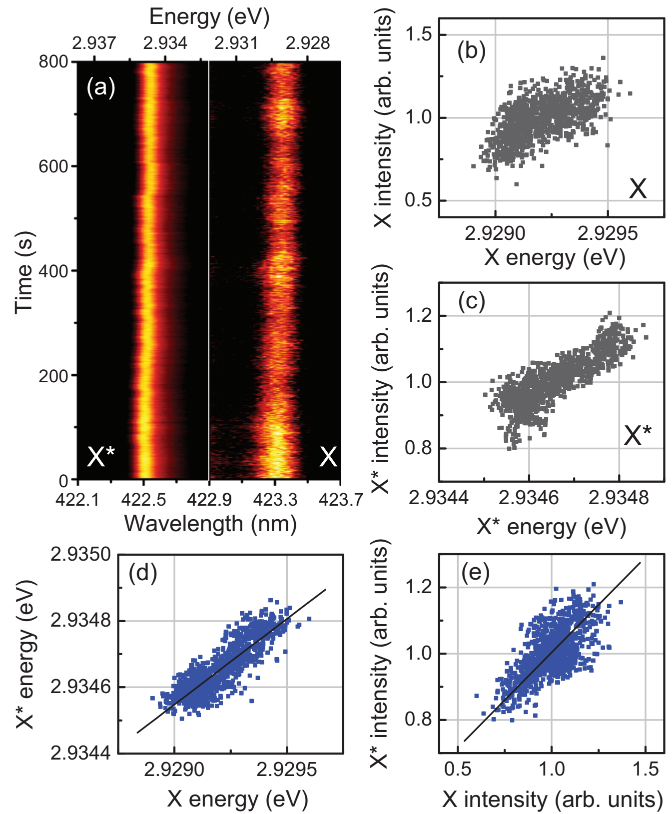

FIG. 4. (Color online) (a) A contour plot of the time evolution of X and X^* lines constructed by consecutive spectra with an integration of 1 s for each. (b) The correlation between the integrated intensity and the peak energy of the X line and (c) the X^* line. (d) The correlation between the peak energies and (e) the integrated intensities of the X and X^* lines. The excitation power used is $P_{ex} = 260\ \mu$W.

Figs. 4(d) and 4(e), where a linear correlation between the peak energies and the intensities of the X^* and X lines are observed, indicating that both lines originate from the same localization center. It is noteworthy that the spectral diffusion amplitudes of the X and X^* lines are of the same order as the excitation-induced energy shifts shown in Fig. 2(c). The X^* line, which is less blueshifted by the excitation power, exhibits a smaller spectral diffusion amplitude. This leads us to conclude that the excitation-dependent energy shifts and the spectral diffusion are all caused by the electric field produced by the nearby charged traps, rather than the screening of the piezoelectric polarization field exhibited in the InGaN/GaN heterostructures.

Time-resolved PL measurements on individual NWs have also been performed and the data are shown in Fig. 5(a). The decay traces can be fitted by a single exponential function with a decay lifetime ranging from 200 to 620 ps. The short recombination lifetime also indicates that the piezoelectric polarization field is negligible in InGaN/GaN NWs, in consistence with the results reported by Bardoux *et al.*[12] In Figs. 5(b) and 5(c), the PL decay traces for the NW ensemble and a sample containing a planar InGaN single QW are displayed. The decay trace for the NW ensemble show a double-exponential decay, which has a faster component with a lifetime ∼400 ps and a slower component with a lifetime

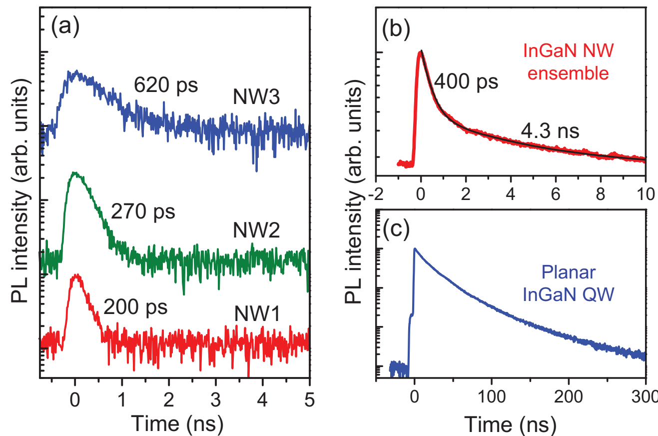

FIG. 5. (Color online) (a) Time-resolved PL traces for localized excitons in three different InGaN/GaN NWs. The decay traces for (b) the NW ensemble and (c) a planar sample containing a single InGaN/GaN QW.

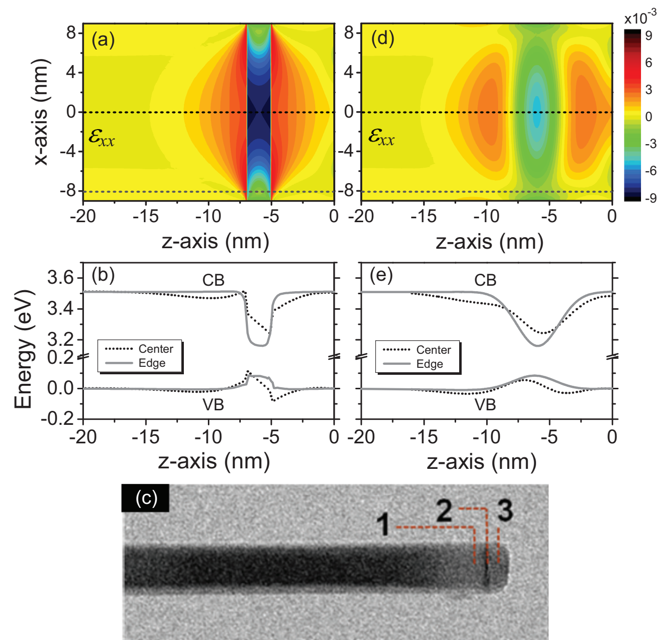

FIG. 6. (Color online) (a) The calculated strain distribution of ϵ_{xx} on the x-z plane for an InGaN/GaN NW with a diameter of 18 nm. (b) The conduction band (CB) and valence band (VB) profiles along the z axis through the disk center (dotted lines) and near the disk edge (solid lines). (c) Composition analysis using STEM-EDX shows that the local In compositions are 2.9%, 10%, and 3.1% when focusing the electron beam on positions 1, 2, and 3, respectively. (d), (e) The calculated strain distribution and the CB and VB potential profiles after considering In-Ga intermixing.

∼4.3 ns. Since the faster decay lifetime is equal to roughly the average value of individual NWs, the faster decay component can be attributed to the recombination of excitons in InGaN localization centers. However, the origin of the slower decay component is not yet clear. A similar double-exponential decay has been reported for InGaN/GaN nanocolumns by Kawakami *et al*. The slower decay component is likely to arise from the recombination of spatially separated electrons and holes in different localization sites in the InGaN layer. A recent study on the recombination dynamics of InGaN/GaN NWs by Cardin *et al.*[30] also leads to a similar conclusion. In contrast to NWs, the decay trace for the conventional QW sample shows a stretched exponential with an initial effective lifetime of ∼20 ns (at which the intensity dropped to $1/e$). The much longer decay lifetime in QW is due to the presence of a large electric field caused by piezoelectric polarizations, which separates the electrons and holes in the QW and hence reduces the oscillatory strength.

According to the experimental results presented above, it is evident that the piezoelectric polarization field in the investigated InGaN/GaN NW heterostructures is *insignificant*. However, recent calculations based on FEM for thicker InGaN/GaN NW heterostructures with diameters of 140 nm (Ref. 14) and ∼50 nm (Refs. 15,16) revealed that the elastic relaxation through the NW geometry is only marginal. To quantify the degree of strain relaxation in thinner NWs investigated here, we have performed FEM simulations[31] for a 2-nm-thick $In_{0.1}Ga_{0.9}N$ disk capped with a 5-nm-thick GaN layer in a GaN NW with a diameter of 18 nm. As shown in Fig. 6(a), the calculated strain ϵ_{xx} in the InGaN disk on the x-z plane is highly nonuniform, which remains almost fully strained (−0.9%) at the disk center and decreases gradually to zero near the NW periphery. This corresponds to a piezoelectric polarization field up to 0.9 MV/cm residing at the center of the disk. This means that, despite NWs with a diameter of only 18 nm, the elastic relaxation via the NW geometry is still inefficient. We have also inspected all the structural analyses for the investigated InGaN/GaN NW heterostructures. From HR-TEM studies,[23] no evidence of misfit dislocations and cracks can be found in the InGaN layer and the vicinal GaN regions. Therefore, plastic relaxations of strain in the InGaN layer can be excluded. In fact, according to Tourbot *et al.*,[32] plastic relaxation is not expected to occur for the low-In-content (∼10%) InGaN disk in thin NWs investigated here.

It has been proposed that localized states in the InGaN layer are inherently insensitive to the electric field due to strong carrier confinements.[16] However, we exclude this reasoning, since the spectral diffusion shown in Fig. 4 indicates that these emission lines are indeed sensitive to the electric field fluctuations.

From the calculated strain distributions, it is likely that carriers are preferentially localized near the periphery of the InGaN disks, where the strain is minimal, leading to the absence of a polarization-induced QCSE. We have also calculated the potential profiles of the conduction band and the valence band along different regions in the NW according to the calculated strain and polarization charges. As shown in Fig. 6(b), the region near the periphery of the InGaN disks shows potential minima and a much weaker piezoelectric polarization field. A similar idea has been proposed by Wu *et al.*,[33] where the PL emission of InGaN/GaN nanorods is suggested to occur near the rod surface. A detailed discussion based on theoretical calculations of an InGaN/GaN NW light-emitting diode can be found in Böcklin *et al.*[34] If the photogenerated carriers are equally likely to be distributed in the highly strained (center) and the fully relaxed (periphery) regions of the InGaN disk, a remarkable QCSE should be

observed in some NWs. However, small excitation-induced energy shifts ($\lesssim$1 meV) and rapid radiative lifetimes (<1 ns) are invariably observed in all the investigated NWs. Indeed, even for much thicker InGaN/GaN NWs with diameters in the range of 40–120 nm in Ref. 11 or 80–150 nm in Ref. 12, where the highly strained area around the disk center is much larger, insignificant QCSEs were still observed. These results thus support the idea that these sharp emission lines mostly originate from carriers localized near the periphery of the InGaN disks, regardless of the NW diameter.

Another possible reason for the suppressed piezoelectric polarization is the alloy intermixing at the InGaN-GaN interfaces. This reasoning comes from the fact that the indium distributions at InGaN-GaN interfaces are not abrupt. This is evident from the composition analysis using STEM-EDX spectroscopy for a NW shown in Fig. 6(c), where the indium composition is found to be 2.9%, 10%, and 3.1% when focusing the electron beam on (1) the bottom GaN region, (2) the InGaN disk layer, and (3) the GaN capping layer, respectively. Such a composition distribution could arise from In-Ga intermixing during the NW growth, especially when a high growth temperature (750 °C) was used for the InGaN layer and the subsequent GaN capping layer. It has been shown that the QCSE depends sensitively on the interface abruptness of the QW structure.[35] In order to quantify the effect of alloy intermixing on the strain distribution, we modeled the composition profile using the standard error function profile in the FEM simulations. The diffusion length is adjusted such that the composition profile matches the STEM-EDX result. The calculated strain distribution and the potential profiles are also shown in Figs. 6(d) and 6(e), respectively. It is clear that the calculated strain at the disk center is reduced considerably. The potential at the InGaN-GaN interfaces is softened by In-Ga intermixing, which can improve the electron-hole wave function overlap and hence reduce the QCSE. Furthermore, both the conduction band and valence band show potential minima near the periphery of the InGaN disk, where the strain and the piezoelectric polarizations are also minimal. This may explain the lack of excitation-induced blueshift and the rapid recombination lifetime for emissions from localization centers in InGaN/GaN NWs.

IV. CONCLUSION

Single InGaN/GaN NWs with a mean diameter down to 18 nm have been investigated by μPL measurements. Sharp emission lines originating from the recombination of localized excitons in the InGaN disk layer can be resolved at low temperatures. Excitation-dependent energy shifts, together with spectral diffusions of these emission lines, indicated a weak QCSE caused by nearby charge fluctuations, rather than the screening of piezoelectric polarizations in the InGaN/GaN heterostructures. The absence of a polarization-induced electric field has been further confirmed by time-resolved PL measurements. Numerical simulations based on FEM indicated that strain relaxation via the NW geometry is inefficient and occurs only near the NW sidewalls. This lead us to suggest that photogenerated carriers might be preferentially localized near the periphery of the InGaN disks, where the strain and piezoelectric polarizations are minimal. Composition analysis based on STEM-EDX combined with FEM simulations reveal that alloy intermixing, which softens the abruptness of the InGaN/GaN interface, may be another reason for the absence of a polarization-induced QCSE in the InGaN/GaN NWs.

ACKNOWLEDGMENT

This work was supported in part by the program of MOE-ATU and the National Science Council of Taiwan under Grant No. NSC-101-2628-M-009-002-MY3.

---

*whchang@mail.nctu.edu.tw

[1] S. Nakamura and S. F. Chichibu, *Introduction to Nitride Semiconductor Blue Lasers and Light Emitting Diodes* (Taylor & Francis, London, 2000).
[2] H. Morkoç, *Handbook of Nitride Semiconductors and Devices* (Wiley, New York, 2008), Vols. I–III.
[3] W. Shan, W. Walukiewicz, E. E. Haller, B. D. Little, J. J. Song, M. D. McCluskey, N. M. Johnson, Z. C. Feng, M. Schurman, and R. A. Stall, J. Appl. Phys. **84**, 4452 (1998).
[4] J. Wu, W. Walukiewicz, K. M. Yu, J. W. Ager, E. E. Haller, H. Lu, and William J. Schaff, Appl. Phys. Lett. **80**, 4741 (2002).
[5] A. Kikuchi, M. Kawai, M. Tada, and K. Kishino, Jpn. J. Appl. Phys. **43**, L1524 (2004).
[6] C.-C. Hong, H. Ahn, C.-Y. Wu, and S. Gwo, Opt. Express **17**, 17227 (2009)
[7] Y.-L. Chang, J. L. Wang, F. Li, and Z. Mi, Appl. Phys. Lett. **96**, 013106 (2010).
[8] H.-W. Lin, Y.-J. Lu, H.-Y. Chen, H.-M. Lee, and S. Gwo, Appl. Phys. Lett. **97**, 073101 (2010).
[9] R. Armitage and K. Tsubaki, Nanotechnology **21**, 195202 (2010).
[10] H. P. T. Nguyen, S. Zhang, K. Cui, X. Han, S. Fathololoumi, M. Couillard, G. A. Botton, and Z. Mi, Nano Lett. **11**, 1919 (2011).
[11] Y. Kawakami, S. Suzuki, A. Kaneta, M. Funato, A. Kikuchi, and K. Kishino, Appl. Phys. Lett. **89**, 163124 (2006).
[12] R. Bardoux, A. Kaneta, M. Funato, Y. Kawakami, A. Kikuchi, and K. Kishino, Phys. Rev. B **79**, 155307 (2009)
[13] M. J. Holmes, Y. S. Park, J. H. Warner, and R. A. Taylor, Appl. Phys. Lett. **95**, 181910 (2009).
[14] M. J. Holmes, Y. S. Park, X. Wang, C. C. S. Chan, A. F. Jarjour, R. A. Taylor, J. H. Warner, J. Luo, H. A. R. El-Ella, and R. A. Oliver, J. Appl. Phys. **109**, 063515 (2011).
[15] M. Knelangen, M. Hanke, E. Luna, L. Schrottke, O. Brandt, and A. Trampert, Nanotechnology **22**, 365703 (2011).
[16] J. Lähnemann, O. Brandt, C. Pfuller, T. Flissikowski, U. Jahn, E. Luna, M. Hanke, M. Knelangen, A. Trampert, and H. T. Grahn, Phys. Rev. B **84**, 155303 (2011).
[17] J. Renard, R. Songmuang, G. Tourbot, C. Bougerol, B. Daudin, and B. Gayral, Phys. Rev. B **80**, 121305(R) (2009).
[18] D. Camacho Mojica and Y.-M. Niquet, Phys. Rev. B **81**, 195313 (2010).

[19] O. Landré, D. Camacho, C. Bougerol, Y. M. Niquet, V. Favre-Nicolin, G. Renaud, H. Renevier, and B. Daudin, Phys. Rev. B **81**, 153306 (2010).
[20] R. Songmuang, D. Kalita, P. Sinha, M. den Hertog, R. André, T. Ben, D. Gonzélez, H. Mariette, and E. Monroy, Appl. Phys. Lett. **99**, 141914 (2011).
[21] S. F. Chichibu, K. Wada, J. Mullhauser, O. Brandt, K. H. Ploog, T. Mizutani, A. Setoguchi, R. Nakai, M. Sugiyama, H. Nakanishi, K. Korii, T. Deguchi, T. Sota, and S. Nakamura, Appl. Phys. Lett. **76**, 1671 (2000).
[22] H. Schömig, S. Halm, A. Forchel, G. Bacher, J. Off, and F. Scholz, Phys. Rev. Lett. **92**, 106802 (2004).
[23] Y.-T. Chen, W.-C. Tsai, W.-Y. Chen, C.-L. Hsiao, H.-C. Hsu, W.-H. Chang, T.-M. Hsu, K.-H. Chen, and L.-C. Chen, Opt. Express **20**, 16166 (2012)
[24] O. Moriwaki, T. Someya, K. Tachibana, S. Ishida, and Y. Arakawa, Appl. Phys. Lett. **76**, 2361 (2000).
[25] M. Senes, K. L. Smith, T. M. Smeeton, S. E. Hooper, and J. Heffernan, Phys. Rev. B **75**, 045314 (2007).
[26] A. F. Jarjour, R. A. Oliver, A. Tahraoui, M. J. Kappers, C. J. Humphreys, and R. A. Taylor, Phys. Rev. Lett. **99**, 197403 (2007).
[27] K. Sebald, J. Kalden, H. Lohmeyer, and J. Gutowski, Phys. Status Solidi B **248**, 1777 (2011).
[28] W.-H. Chang, H.-S. Chang, W.-Y. Chen, T. M. Hsu, T.-P. Hsieh, J.-I. Chyi, and N.-T. Yeh, Phys. Rev. B **72**, 233302 (2005).
[29] C. Y. Lai, T. M. Hsu, W.-H. Chang, K.-U. Tseng, C.-M. Lee, C.-C. Chuo, and J.-I. Chyi, J. Appl. Phys. **91**, 531 (2002).
[30] V. Cardin, L. I. Dion-Bertrand, P. Grégoire, H. P. T. Nguyen, M. Sakowicz, Z. Mi, C. Silva, and R. Leonelli, Nanotechnology **24**, 045702 (2013).
[31] Numerical calculations were performed using the next**nano**^{3} three-dimensional (3D) nanodevice simulator.
[32] G. Tourbot, C. Bougerol, A. Grenier, M. Den Hertog, D. Sam-Giao, D. Cooper, P. Gilet, B. Gayral, and B. Daudin, Nanotechnology **22**, 075601 (2011).
[33] Y.-R. Wu, C. Chiu, C.-Y. Chang, P. Yu, and H.-C. Kuo, IEEE J. Sel. Top. Quantum Electron. **15**, 1226 (2009).
[34] C. Böcklin, R. G. Veprek, S. Steiger, and B. Witzigmann, Phys. Rev. B **81**, 155306 (2010).
[35] J. A. Davis, L. V. Dao, X. Wen, C. Ticknor, P. Hannaford, V. A. Coleman, H. H. Tan, C. Jagadish, K. Koike, S. Sasa, M. Inoue, and M. Yano, Nanotechnology **19**, 055205 (2008).